SOLAR PHYSICS

# On the generation of solar spicules and Alfvénic waves

J. Martínez-Sykora,[1,2]* B. De Pontieu,[2,3] V. H. Hansteen,[3,2] L. Rouppe van der Voort,[3] M. Carlsson,[3] T. M. D. Pereira[3]

**In the lower solar atmosphere, the chromosphere is permeated by jets known as spicules, in which plasma is propelled at speeds of 50 to 150 kilometers per second into the corona. The origin of the spicules is poorly understood, although they are expected to play a role in heating the million-degree corona and are associated with Alfvénic waves that help drive the solar wind. We compare magnetohydrodynamic simulations of spicules with observations from the Interface Region Imaging Spectrograph and the Swedish 1-m Solar Telescope. Spicules are shown to occur when magnetic tension is amplified and transported upward through interactions between ions and neutrals or ambipolar diffusion. The tension is impulsively released to drive flows, heat plasma (through ambipolar diffusion), and generate Alfvénic waves.**

Spicules are ubiquitous, highly dynamic jets of plasma that are observed at the solar limb (*1*–*3*). Recent observations indicate that in most of these jets (type II spicules), initially cool (~$10^4$ K) plasma is accelerated into the corona at speeds of up to 150 km $s^{-1}$. A substantial fraction of the ejected plasma is heated to temperatures typical of the solar transition region [TR, >$10^4$ K (*3*–*5*); this narrow region separates the cool chromosphere from the hot corona] before falling back to the surface after 5 to 10 min. Spicules may play a critical role in energizing the outer solar atmosphere and have been suggested as a source of hot plasma to the corona [(*6*), but see (*7*)], potentially helping explain its puzzling temperatures of several million degrees. Spicules carry a large flux of Alfvénic waves (*8*–*10*) that may help drive the solar wind and/or heat the corona (*11*). Despite major observational advances, the generation of type II spicules remains poorly understood: Although there are suggestions that magnetic reconnection plays a role (*6*), there are no models at present (*12*) that can explain all of the observed properties of type II spicules, including their ubiquity (*3*–*5*) and the strong magnetic waves that they carry (*8*, *9*, *13*).

We present 2.5-dimensional (2.5D) radiative magnetohydrodynamic (MHD) numerical simulations in which spicule-like features naturally and frequently occur. Our model captures the complex physical processes that play a role in spicule formation and evolution: (i) Plasma is not in local thermodynamic equilibrium; (ii) radiation is optically thick and undergoes scattering; (iii) gas is partially ionized; and (iv) thermal conduction is important in the upper chromosphere, TR, and corona (supplementary materials). Although previous numerical experiments included many of these processes (*12*), they did not produce any (*14*) or produced only a few (*15*) features that resembled type II spicules because they lacked ambipolar diffusion (supplementary text). We find that high spatial resolution (<40 km), large-scale magnetic field (e.g., magnetic loops ~50 Mm long), and ion-neutral interaction effects in the partially ionized chromosphere are critical for the ubiquitous formation of spicules. Our results show that spicule-like jets occur frequently in the vicinity of strong magnetic flux concentrations (e.g., the positions 20, 40, and 70 Mm on the horizontal axis in Fig. 1 and movie S1) that are similar to so-called plage regions (large concentrations of magnetic flux with predominantly one polarity). We can identify at least two different drivers for type II spicules in the model. One (described below) is much more frequent than the other (described in the supplementary materials).

Several steps are required for the formation of spicule-like features. First, convective motions in the photosphere distort the magnetic field in the vicinity of strong vertical magnetic flux concentrations. This occurs through the interaction of these vertical concentrations with neighboring horizontal fields associated with weaker, granular-scale flux concentrations (left panels, Fig. 2). In an environment in which plasma β (the ratio of plasma to magnetic pressure) is high (i.e, gas pressure greater than magnetic pressure), this interaction can lead to the local buildup of strong magnetic tension. In our simulations, such weak fields continuously appear as a result of processing and shredding of strong fields caused by convective motions. These conditions are likely to be found frequently on the Sun in the vicinity of regions that are dominated by mostly vertical magnetic flux concentrations of several kilogauss, such as the magnetic network (in the quiescent Sun) or plage (in active regions). These are surrounded by weak, mostly horizontal flux that continuously emerges on granular scales of ~$10^3$ km (*16*).

Next, this region of highly bent magnetic field and thus large magnetic tension must move into the upper chromosphere, where the magnetic field dominates the plasma (β < 1). However, weak horizontal fields are typically not buoyant enough to emerge into the atmosphere (*17*). The process that allows this region of magnetic tension to move to greater heights is ambipolar diffusion, which arises from slippage between the ions and neutral particles in the partially ionized chromosphere. The ambipolar diffusion allows magnetic field to move through neutral particles, and the collisions between neutrals and ions can lead to magnetic energy dissipation. Ambipolar diffusion depends on the ion-neutral collision frequency and magnetic field strength, which is largest in the coldest parts of the chromosphere and affects the emergence of regions with high magnetic tension in two ways: (i) Sporadically, ambipolar diffusion becomes large just above the photosphere as a result of the strong expansion and adiabatic cooling in the wake of magneto-acoustic shocks that propagate upward. When this happens close to a region of high magnetic tension, the ion-neutral interaction diffuses the mostly horizontal upper photospheric fields into the chromosphere, allowing the highly bent magnetic field to penetrate upward into a low-plasma-β regime. (ii) The emergence into the chromosphere leads to expansion

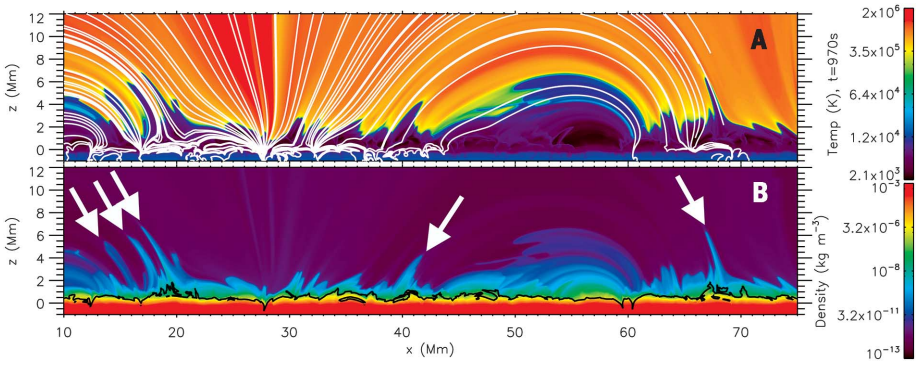


**Fig. 1. Spicule-like features (indicated by arrows) occur in our radiative MHD simulations.** They appear as dense, cool intrusions in the hot corona, originating from the boundaries of the strong magnetic regions. (**A**) Temperature and (**B**) density maps are shown on a logarithmic color map with white magnetic field lines (A) and black contours where plasma β = 1 (B). *t*, time.

[1]Bay Area Environmental Research Institute, Petaluma, CA 94952, USA. [2]Lockheed Martin Solar and Astrophysics Laboratory (LMSAL), Palo Alto, CA 94304, USA. [3]Institute of Theoretical Astrophysics, University of Oslo, Post Office Box 1029, Blindern, N-0315 Oslo, Norway.
*Corresponding author. Email: juanms@lmsal.com

of the field, which in turn leads to cooling and a dramatic increase in ambipolar diffusion within the emerging region. As a result, any current perpendicular to the field lines (Fig. 2, M to P, and movie S2) is partially dissipated in the cold expanding pockets and partially advected to the sides of the cold regions, where the ambipolar diffusion is lower (Fig. 2, I to L). This current leads to a further amplification of the magnetic tension and its concentration into a narrower layer at the boundaries of the emerging flux bubble.

In the final step, the magnetic tension is violently released in the upper chromosphere, which drives strong flows (~100 km $s^{-1}$; Fig. 2, E to H). The magnetic field releases its tension by retracting and straightening, similar to the whiplash effect during magnetic reconnection (*18*). The straightening field squeezes the plasma in a confined region, which produces, through pressure gradients, a strong acceleration of the chromospheric plasma to high speeds along the ambient magnetic field. The whiplash effect also generates Alfvénic waves that rapidly propagate upward, as well as electrical currents.

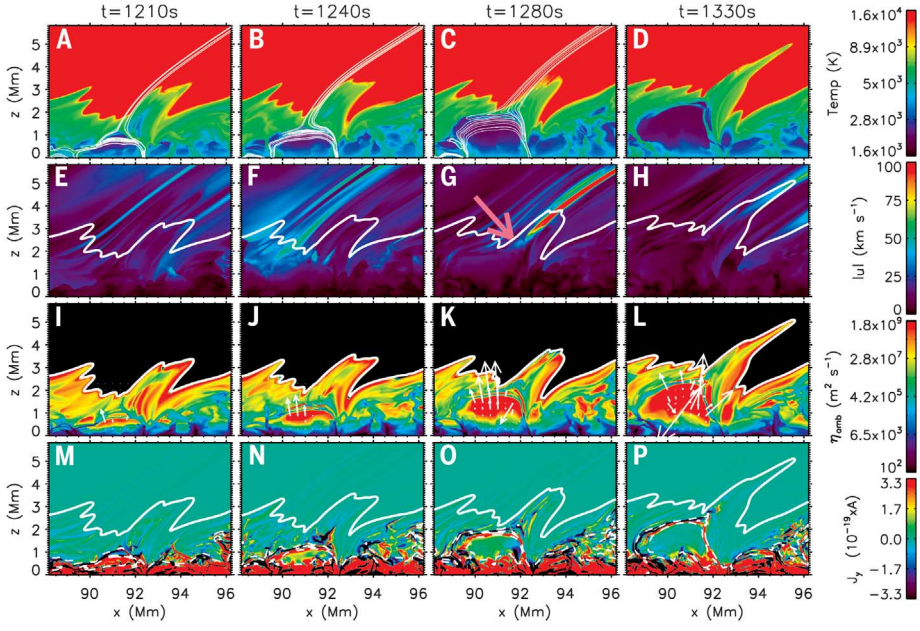


**Fig. 2. Spicules form when strong magnetic tension is diffused into the upper chromosphere, where its release drives strong flows, heating, and Alfvénic waves.** (**A** to **P**) A time series is shown of temperature, absolute velocity (|u|), ambipolar diffusion ($\eta_{amb}$), and current perpendicular to the plane ($J_y$). The thick white contour is at $10^5$ K in (E) to (P). The region of strong tension is illustrated in (A) to (C) with white magnetic field lines. The fully formed spicule is shown in the rightmost panels. White arrows in (I) to (L) show ambipolar velocities leading to upward diffusion of the high-tension region. Strong ambipolar diffusion in the expanding emerging flux bubble at $t$ = 1280 s concentrates the perpendicular current at the edges of the bubble, amplifying the tension. Pink contours in (G) show locations of a strong plasma pressure gradient (driving spicular flows upward) resulting from the release of magnetic tension (pink arrow).

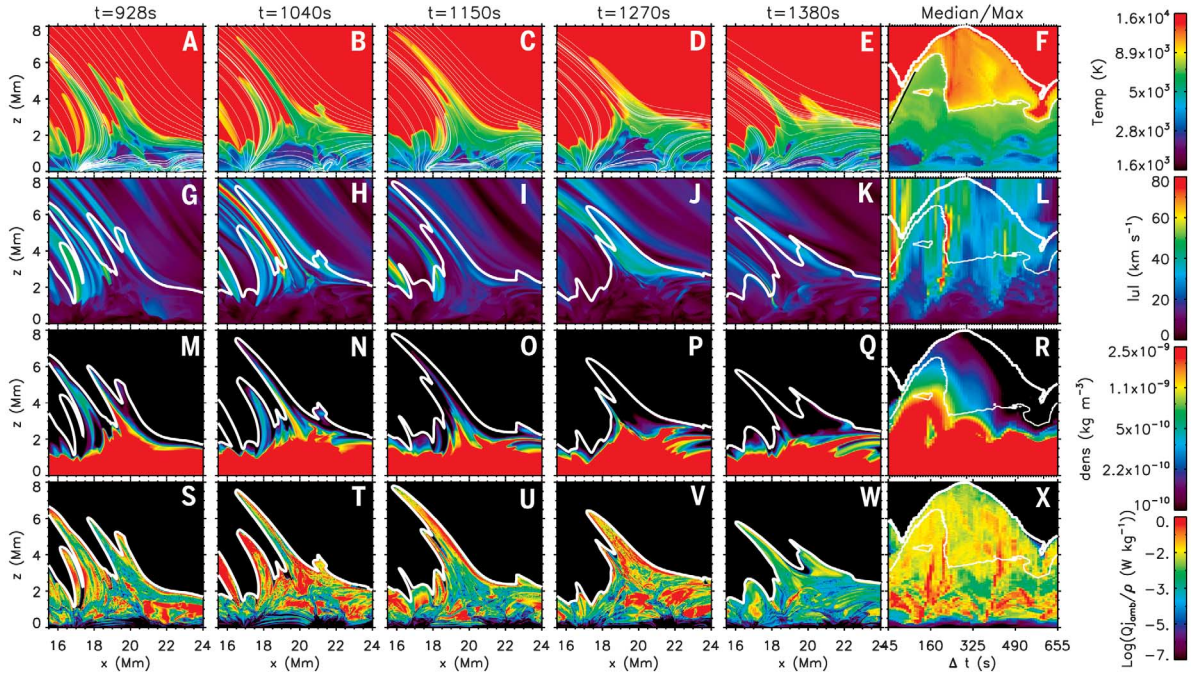


**Fig. 3. Heating of spicules from dissipation of electrical currents through ambipolar diffusion.** (**A** to **X**) Time series of maps of temperature, absolute velocity, density, and Joule heating per particle from ambipolar diffusion (where $Qj_{amb}$ is Joule heating per volume and ρ is density). The median temperature (F), maximum velocity (L), median density (R), and median Joule heating per particle from ambipolar diffusion (X) within the spicule (<$10^5$ K) are shown as a function of time and height. Magnetic field lines are in white in (A) to (E), and the thick white contour is at $10^5$ K in the three bottom rows. The rightmost column includes a thin contour at 8 × $10^3$ K.

Our simulation reproduces many observed properties of type II spicules (Fig. 3 and movie S3), including highly collimated and strong flows (~100 km $s^{-1}$) that reach heights up to 10 Mm (*4*, *19*) within a lifetime of 2 to 10 min (*5*). The vertical motion of the TR above the spicule peaks at 30 to 35 km $s^{-1}$, which translates to an apparent motion along the spicule of ~40 to 45 km $s^{-1}$ (Fig. 3F) when taking into account the inclination, in agreement with observed apparent motions along spicules at the solar limb (*4*). Our model predicts spicules to occur in the vicinity of the network and plage regions, especially toward the periphery of strong flux regions, where interactions with weaker flux can easily occur. Our simulation shows a much higher spicule occurrence rate than previous studies (*15*), which produced only two examples. Although those two spicule-like features were also propelled by magnetic tension, the simulations lacked ambipolar diffusion, and the underlying driver was injection of strong field at the lower boundary. These earlier 3D simulations did not reproduce many observed properties of spicules (*12*). However, the similarities of the driving mechanism in the 3D simulations suggest that the 2.5D limitation of our simulations does not meaningfully affect our results. This is also supported by the highly collimated nature of the flows and shocks in our simulations (discussed below and in the supplementary materials).

Our model predicts heating from chromospheric (<$10^4$ K) to TR (>$2 \times 10^4$ K) temperatures during the evolution of the spicules (Fig. 3 and movie S3). Currents driven by the whiplash effect are partially dissipated (Fig. 2, M to P) through ambipolar diffusion, thereby heating the chromospheric spicular plasma to at least TR temperatures within 2 min during its expansion into the corona (Fig. 3, S to X). This is compatible with observations that show a relatively short (<1.5 min), cool [visible in the CaII lines] initial phase, followed by a longer-lived phase (~5 to 10 min) at higher temperatures (visible in MgII and SiIV lines) (*5*). In the model, the remaining currents penetrate into the corona and are dissipated via Joule heating, and the connected magnetic loops and spicule-associated plasma reach coronal temperatures of 2 MK (Figs. 2 and 4 and movie S2).

We generated synthetic observations of the spicules in our simulation for comparison with observations from the Swedish 1-m Solar Telescope (SST) (*20*) and NASA's Interface Region Imaging Spectrograph (IRIS) (*21*). We compared the CaII 8542 Å (middle chromosphere, ~$8 \times 10^3$ K), MgII h 2803 Å (upper chromosphere, ~1 to $1.5 \times 10^4$ K), SiIV 1402 Å (~$8 \times 10^4$ K), and FeIX 171 Å (~1 MK) spectral lines (Fig. 4). The model reproduces the short lifetimes (<1 min) of high-velocity excursions in the blue wing of chromospheric lines such as CaII 8542 Å and MgII h 2803 Å—the so-called rapid blueshifted events (RBEs) that are the disk counterparts of type II spicules (*22*, *23*). The strong upward velocities at chromospheric temperatures (Fig. 3, G to L, and movie S3) last for only a few tens of seconds. The density along the spicule decreases with time (Fig. 3, M to R, and movie S3), which contributes to the short lifetime in chromospheric lines. The TR counterparts of the model spicules are visible as strong blueshifted excursions of the $Si^{IV}$ line, which agrees well with IRIS observations (Fig. 4, C and G). The modeled spicule also presents a signal in the coronal $Fe^{IX}$ 171 Å line, similar to what has been observed before (*24*).

Our simulation indicates that spicules may play a substantial role in energizing the outer solar atmosphere, by supplying plasma to the corona and by the generation of strong electrical currents and Alfvénic waves. Assuming that the spicules have widths of 300 km in all directions, a spicule supplies ~$10^{10}$ kg of hot plasma to the corona per event. The strong intermittent currents that are an integral driving component of spicules fill the spicule and propagate into the corona. These currents are dissipated by the ambipolar diffusion in chromospheric or spicular plasma, which leads to substantial heating on the order of ~$10^{18}$ J per event (integrated over the spicule lifetime). Ambipolar diffusion is not effective at coronal temperatures, but these spicule-associated currents also have clear potential for heating plasma in the coronal volume (*25*, *26*). This is illustrated by the hot coronal loops that appear in association with the simulated spicules, which are filled and heated by current dissipation (in our simulation by artificial diffusion; supplementary materials), strong flows and shocks, evaporation, and thermal conduction.

Alfvénic motions have additional capacity for heating plasma to coronal temperatures (*11*). The Alfvénic motions that are generated through the whiplash effect lead to transverse waves in our 2.5D simulations and would lead to torsional and kink waves on the Sun. In our simulation, the average amplitude for these waves is 20 km $s^{-1}$, and we estimate (supplementary materials) that the average energy flux is ~$10^3$ W $m^{-2}$ in the spicule and ~300 W $m^{-2}$ in the lower corona, which is comparable to observations (*8*, *9*). Dissipation of such waves (e.g., through resonant absorption) is not properly treated by our simulation because it does not include the small spatial scales on which such mode-coupling and subsequent Kelvin Helmholtz instability vortices occur, but wave dissipation can also lead to substantial heating of the outer atmosphere (*11*, *27*–*29*).

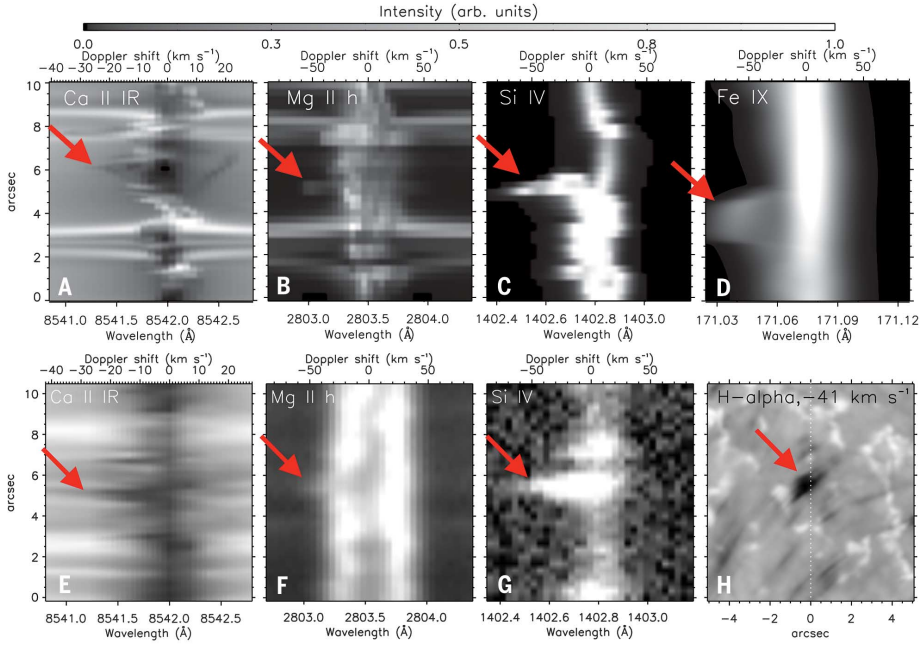


**Fig. 4. Synthetic observations of a simulated spicule compared with observations from the Swedish 1-m Solar Telescope (SST) and the Interface Region Imaging Spectrograph (IRIS).** (**A** to **D**) Wavelength-space plots of synthetic observations of CaII 8542 Å (middle chromosphere), MgII h 2803 Å (upper chromosphere), SiIV 1403 Å (transition region), and FeIX 171 Å (corona). The spicular signal appears as a blueward excursion around 3 to 6 arc sec (red arrows). The signals are offset spatially because the spicule is inclined from the vertical. (**E** to **H**) A disk observation of a spicule (or RBE) in CaII 8542 Å (SST), MgII h 2803 Å (IRIS), and SiIV 1403 Å (IRIS), and a map of the blue wing (−41 km $s^{-1}$) of Hα 6563 Å (SST). The white dotted line in (H) indicates the location of the IRIS slit. The spatial range in (A) to (D) corresponds to the region shown in Fig. 3 at $t$ = 929 s.

## REFERENCES AND NOTES


1. A. Secchi, *Die Sterne: Grundzuge der Astronomie der Fixsterne* (Brockhaus, 1878).
2. G. Tsiropoula *et al.*, *Space Sci. Rev.* **169**, 181–244 (2012).
3. B. De Pontieu *et al.*, *Publ. Astron. Soc. Jpn.* **59**, S655 (2007).
4. T. M. D. Pereira, B. De Pontieu, M. Carlsson, *Astrophys. J.* **759**, 18 (2012).
5. T. M. D. Pereira *et al.*, *Astrophys. J.* **792**, L15 (2014).
6. B. De Pontieu *et al.*, *Science* **331**, 55–58 (2011).
7. J. A. Klimchuk, S. J. Bradshaw, *Astrophys. J.* **791**, 60 (2014).

8. B. De Pontieu *et al.*, *Science* **318**, 1574–1577 (2007).
9. S. W. McIntosh *et al.*, *Nature* **475**, 477–480 (2011).
10. B. De Pontieu, A. Title, M. Carlsson, *Science* **346**, 315 (2014).
11. J. V. Hollweg, *J. Goephys. Res.* **91**, 4111 (1986).
12. J. Martínez-Sykora *et al.*, *Astrophys. J.* **771**, 66 (2013).
13. B. De Pontieu *et al.*, *Astrophys. J.* **752**, L12 (2012).
14. M. Carlsson, V. H. Hansteen, B. V. Gudiksen, J. Leenaarts, B. De Pontieu, *Astron. Astrophys.* **585**, A4 (2016).
15. J. Martínez-Sykora, V. Hansteen, F. Moreno-Insertis, *Astrophys. J.* **736**, 9 (2011).
16. B. W. Lites *et al.*, *Astrophys. J.* **672**, 1237–1253 (2008).
17. D. J. Acheson, *Sol. Phys.* **62**, 23–50 (1979).
18. T. Yokoyama, K. Shibata, *Publ. Astron. Soc. Jpn.* **48**, 353–376 (1996).
19. L. Rouppe van der Voort, J. Leenaarts, B. de Pontieu, M. Carlsson, G. Vissers, *Astrophys. J.* **705**, 272–284 (2009).
20. G. B. Scharmer, K. Bjelksjo, T. K. Korhonen, B. Lindberg, B. Petterson, *Proc. SPIE Conf. Ser.* **4853**, 341 (2003).
21. B. De Pontieu *et al.*, *Sol. Phys.* **289**, 2733–2779 (2014).
22. D. H. Sekse, L. Rouppe van der Voort, B. De Pontieu, *Astrophys. J.* **752**, 108 (2012).
23. L. Rouppe van der Voort, B. de Pontieu, T. M. D. Pereira, M. Carlsson, V. H. Hansteen, *Astrophys. J.* **799**, L3 (2015).
24. B. De Pontieu, S. W. McIntosh, V. H. Hansteen, C. J. Schrijver, *Astrophys. J.* **701**, L1–L6 (2009).
25. E. N. Parker, *Sol. Phys.* **121**, 271 (1989).
26. V. H. Hansteen, N. Guerreiro, B. D. Pontieu, M. Carlsson, *Astrophys. J.* **811**, 106 (2015).
27. P. Antolin *et al.*, *Astrophys. J.* **809**, 72 (2015).
28. J. Okamoto, B. De Pontieu, *Astrophys. J.* **736**, L24 (2011).
29. J. Okamoto *et al.*, *Astrophys. J.* **809**, 71 (2015).

## ACKNOWLEDGMENTS

This work is supported by NASA, the Research Council of Norway, and the European Research Council (ERC). IRIS is a NASA Small Explorer mission developed and operated by LMSAL with mission operations executed at NASA Ames Research Center and major contributions to downlink communications funded by the European Space Agency and the Norwegian Space Centre. The SST is operated on the island of La Palma by the Institute for Solar Physics of Stockholm University in the Spanish Observatorio del Roque de los Muchachos of the Instituto de Astrofísica de Canarias. We gratefully acknowledge support by NASA grants NNX11AN98G, NNM12AB40P, NNH15ZDA001N-HSR, and NNX16AG90G and NASA contracts NNM07AA01C (Hinode) and NNG09FA40C (IRIS). This research was supported by the Research Council of Norway and by the ERC under the European Union's Seventh Framework Programme (FP7/2007–2013; ERC grant agreement no. 291058). The simulations were run on clusters from the Notur project and the Pleiades cluster through computing project s1061 from NASA's High-End Computing Program. We thankfully acknowledge the computer and supercomputer resources of the Research Council of Norway through grant 170935/V30 and through grants of computing time from the Programme for Supercomputing. IRIS observations are archived at http://iris.lmsal.com/data.html; level 3 data including the SST and IRIS observations used for Fig. 4 are accessible at http://bit.ly/2mnGVYg. The simulation output and synthetic observables for models B and C are available at http://sdc.uio.no/search/simulations under the names en096014_gol and en096014_nongol, respectively. Executables for the Bifrost software and files necessary to run the simulations are available at http://iris.lmsal.com/bf/code.tar.bz2, source code for RH is at http://github.com/ITA-Solar/rh, (supplementary materials) and the optically thin radiation was calculated using the IRIS library of SolarSoft at www.lmsal.com/solarsoft/. Various items of documentation for these software and output files are available at http://iris.lmsal.com/modeling.html.

## SUPPLEMENTARY MATERIALS

www.sciencemag.org/content/356/6344/1269/suppl/DC1
Materials and Methods
Supplementary Text
Figs. S1 to S6
Table S1
References (*30*–*69*)
Movies S1 to S5

11 July 2016; accepted 26 May 2017
10.1126/science.aah5412

# On the generation of solar spicules and Alfvénic waves

J. Martínez-Sykora, B. De Pontieu, V. H. Hansteen, L. Rouppe van der Voort, M. Carlsson and T. M. D. Pereira

*Science* **356** (6344), 1269-1272.
DOI: 10.1126/science.aah5412

**Understanding the formation of spicules**

Spicules are small jets lasting a few minutes that form in the solar atmosphere and propel hot plasma upward from the visible surface. The underlying physics of spicules is not well understood. Martínez-Sykora *et al.* developed radiation-magnetohydrodynamic simulations that can spontaneously produce numerous spicules with properties that match observations. Interactions between large-scale magnetic fields and the plasma, such as ambipolar diffusion, drive the formation process and subsequent evolution. Understanding how spicules form will help assess how much they heat the solar corona and how they relate to other solar phenomena.

*Science*, this issue p. 1269